Chinese Physics Letters

LETTER

# Two-Electron Correlations in the Metallic Electron Gas

Cite as: Zhiyi Li *et al*. 2026 *Chin. Phys. Lett.* **43** 080705

DOI CSTR

## Recommended Articles

**Electronic Structure of a Correlated Antiferromagnetic Metal CrN in Epitaxial Thin Film Form**
Rui Xu, Jiexiong Sun, Tongrui Li, Jianghao Yao, Yuzhe Wang, Xianglin Li, Shiwu Su, Donglai Feng, and Juan Jiang
*Chin. Phys. Lett.* **43**, 060711 (2026)

**Comment on "Superconductivity in Kagome Metal $YRu_3Si_2$ with Strong Electron Correlations"**
Evgeny F. Talantsev
*Chin. Phys. Lett.* **43**, 060706 (2026)

**Spin-Polarized Two-Dimensional Electron Gas with Giant Rashba Splitting at the $EuTiO_3/KTaO_3(111)$ Interface under Light Illumination**
Yu-Chen Zhao *et al*.
*Chin. Phys. Lett.* **42**, 100703 (2025)

**h-BN-assisted Metal Contact Transfer to InSe for Two-Dimensional Multifunctional Electronic Devices**
Chijun Wei, Nuertai Jiazila, Xuanye Liu, Peng Song, Hui Gao, Jiequn Sun, Lihong Bao, Xiao Lin, and Hong-Jun Gao
*Chin. Phys. Lett.* **41**, 128501 (2024)

**Many-Body Enhancement of Excitonic Electron–Hole Recombination in Two-Dimensional Transition Metal Dichalcogenides**
Li Yao, Xiang Jiang, Qijing Zheng, and Jin Zhao
*Chin. Phys. Lett.* **43**, 010701 (2026)

**Electronic Correlation and Pseudogap-Like Behavior of High-Temperature Superconductor $La_3Ni_2O_7$**
Yidian Li *et al*.
*Chin. Phys. Lett.* **41**, (2024)

A series journal of Chinese Physical Society distributed by IOP Publishing

Chinese Physics Letters

*Chin. Phys. Lett.* **43** 080705 (2026)

LETTER

DOI: 10.1088/0256-307X/43/8/080705
CSTR: 32039.14.0256-307X.43.8.080705

# Two-Electron Correlations in the Metallic Electron Gas

**Zhiyi Li[1,2,†], Pengcheng Hou[2,†], Bao-Zong Wang[3,*], Youjin Deng[1,2,4,*], and Kun Chen[5,*]**

[1]Department of Modern Physics, University of Science and Technology of China, Hefei 230026, China
[2]Hefei National Laboratory, University of Science and Technology of China, Hefei 230088, China
[3]International Center for Quantum Materials, School of Physics, Peking University, Beijing 100871, China
[4]Hefei National Research Center for Physical Sciences at the Microscale and School of Physical Sciences, University of Science and Technology of China, Hefei 230026, China
[5]CAS Key Laboratory of Theoretical Physics, Institute of Theoretical Physics, Chinese Academy of Sciences, Beijing 100190, China

[†]These authors contributed equally to this work.
[*]Corresponding authors. Email: bzwang.phys@gmail.com; yjdeng@ustc.edu.cn; chenkun@itp.ac.cn

**We present high-precision *ab initio* calculations of the four-point vertex function for the three-dimensional uniform electron gas using variational diagrammatic Monte Carlo. From these results, we extract Landau parameters that reveal a density-driven crossover from underscreening to overscreening, and obtain the full two-electron scattering amplitude on the Fermi surface with controlled accuracy. A residual analysis of the scattering amplitude against the charge-channel Kukkonen−Overhauser ($KO^+$) interaction shows that only a minimal s-wave correction in the antiparallel-spin channel is needed, defining the $sKO^+$ ansatz: $KO^+$ within the local-density approximation plus this short-range correction. Using both our direct VDMC amplitudes and the $sKO^+$ ansatz, we compute the electron–electron contribution to the thermal resistivity, obtaining quantitative agreement with experiments on simple metals (Al, Na, K, Rb). $sKO^+$ thus provides a controlled UEG-based effective interaction for simple-metal transport and future first-principles extensions.**

## Introduction

The collective behavior of interacting electrons gives rise to some of the most profound and challenging problems in condensed matter physics [1], including high-temperature superconductivity [2], strange metallicity [3], and the emergence of topological phases [4]. The uniform electron gas (UEG)—an idealized model of electrons moving in a uniform neutralizing background—provides the quintessential canvas for understanding correlations originating solely from the Coulomb interaction [5]. While the single-particle properties of this system have been extensively studied [6], a comprehensive understanding of two-electron correlations has remained elusive despite their fundamental importance.

Two-electron correlations on the Fermi surface are encoded in the four-point vertex function, which simultaneously controls Fermi-liquid parameters [7,8], pairing instabilities [9], and the electron–electron scattering rates that govern transport phenomena [10]. A first-principles determination has historically been impeded by its complex dependence on multiple momentum and frequency variables. The immense computational cost associated with this high dimensionality poses a severe challenge, forcing many theoretical frameworks to rely on approximations, such as low-order truncations in diagrammatic methods or the local approximations in dynamical mean-field extensions and post-GW schemes [11−14]. Conventional quantum Monte Carlo (QMC) techniques face a complementary limitation. They accurately access ground-state energies and selected correlations, but not the vertex function directly. Extracting it requires four-point correlations that are difficult to resolve with sufficient accuracy in standard QMC. This theoretical gap is particularly pressing today, as advances in two-electron photoemission and multidimensional electronic spectroscopies begin to access many-electron correlations experimentally [15−17].

The consequences of this theoretical gap are particularly stark in the study of transport phenomena, presenting a long-standing challenge to the first-principles description of thermal conductivity in simple metals. Here, electron–electron scattering is understood to be a primary contributor to the experimentally observed deviations from the Wiedemann–Franz law [21−26], an effect that conventional density functional theory (DFT) struggles to account for Ref. [27]. Previous attempts to resolve this issue using many-body theories, such as the random phase approximation (RPA) [28,29] and the Kukkonen–Overhauser (KO) interaction [20,30], have also resulted in thermal resistivity values that disagree with experimental measurements. Consequently, finding a theoretical ansatz for the effective electron–electron interaction that yields precise quantitative agreement with experiment remains an open challenge and makes this problem directly relevant to transport theory and experiments in simple metals.

In this work, we address this challenge using the variational

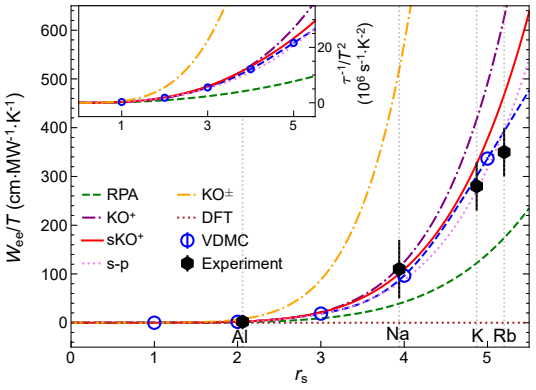


**Fig. 1.** The electron–electron contribution to the thermal resistivity $W_{ee}$ as a function of density parameter $r_s$ in the metallic regime, computed from our variational diagrammatic Monte Carlo (VDMC) results (blue circles) and from several theoretical models, including the random phase approximation (RPA), the s–p approximation [18,19], the original Kukkonen–Overhauser interaction [20] ($KO^\pm$), and the charge-channel-only form ($KO^+$). For comparison, we plot experimental data (black circles) for simple metals [21−24]. The solid red line shows our proposed $sKO^+$ model, namely $KO^+$ supplemented by s-wave corrections, which agrees well with the VDMC results and experimental measurements. The inset shows the electron–electron scattering rate.

Received 25 April 2026; accepted 7 July 2026; published 26 August 2026
© 2026 Chinese Physical Society and IOP Publishing Ltd. All rights, including for text and data mining, AI training, and similar technologies, are reserved.

Check for updates

diagrammatic Monte Carlo (VDMC) method [31–34], which combines a variational principle with high-order, controlled stochastic summation of Feynman diagrams [35–45]. For the 3D UEG, we compute the four-point vertex up to sixth order, comprehensively characterizing two-electron correlations and extracting the Landau parameters $F^{\mathrm{s,a}}_{0,1,2}$. This provides a long-sought, first-principles quantitative determination of these key Fermi-liquid parameters. Our results reveal a crossover from underscreening to overscreening [46–48], where collective screening drives the static dielectric function negative, effectively inverting the test-charge interaction from repulsive to attractive. This transition is characterized by the Landau parameter $F^{\mathrm{s}}_0$ approaching $-1$, signaling a divergence in electronic compressibility and the onset of a strongly correlated regime.

Furthermore, we calculate the full electron–electron scattering amplitude with high precision across the entire Fermi surface. Guided by these numerical results, we introduce the following effective interaction:

$$R^{\sigma\sigma'}_{\boldsymbol{k}_1\boldsymbol{k}_2\boldsymbol{q}} = \frac{v_q + f^{+}_{\mathrm{XC}}}{1-[v_q+f^{+}_{\mathrm{XC}}]\Pi_0(q)} - f^{+}_{\mathrm{XC}} + \delta R^{\sigma\sigma'},$$
$$\delta R^{\sigma\sigma'} = (1-\delta_{\sigma\sigma'})\left[C_0 + C_2\frac{(\boldsymbol{k}_1-\boldsymbol{k}_2)^2+(\boldsymbol{k}_1-\boldsymbol{k}_2-2\boldsymbol{q})^2}{2}\right]. \quad (1)$$

Here $f^{+}_{\mathrm{XC}}$ denotes the symmetric exchange-correlation (XC) kernel. The XC kernels discussed in this work are treated within LDA by replacing $f^{\pm}_{\mathrm{XC}}(q)$ with their static, long-wavelength values $f^{\pm}_{\mathrm{XC}}(0)$. Specifically, this ansatz is constructed by starting from the charge-channel KO interaction and adding a small s-wave correction $\delta R$ acting only in the antiparallel-spin channel, parametrized by $C_0$ and $C_2$ and associated with the s-wave scattering length and effective range. By setting $\delta R = 0$, equation (1) recovers the charge-channel KO model, KO$^+$. This ansatz resolves the discrepancies found in widely used approximations such as RPA and KO. It provides a quantitatively accurate effective interaction on the Fermi surface, extending naturally to finite momentum through the closed-form structure inherited from KO$^+$.

Crucially, our first-principles results for the electron–electron scattering amplitude enable a direct calculation of the thermal resistivity, resolving the long-standing discrepancy between previous theoretical approximations and experimental measurements. As shown in Fig. 1, the resistivity derived from our calculated scattering amplitude is in good agreement with experimental data [21–24]. Moreover, the thermal resistivity calculated using our proposed sKO$^+$ model also closely matches the experimental values, confirming the validity of our comprehensive approach. Beyond this validation, the closed-form sKO$^+$ provides a UEG-based input for downstream first-principles methods, with concrete applications to time-dependent DFT (TDDFT) kernels, Eliashberg- and Boltzmann-type transport calculations, and effective-field-theory constructions discussed below.

## Methods

We employ the VDMC framework [31–41], which combines a robust variational principle with stochastic sampling of Feynman diagrams. This approach enables controlled evaluation of high-order perturbative contributions to the four-point vertex function of the UEG.

The microscopic model is the standard UEG Hamiltonian

$$H = \sum_{\boldsymbol{k}\sigma}(\boldsymbol{k}^2-\mu)\psi^{\dagger}_{\boldsymbol{k}\sigma}\psi_{\boldsymbol{k}\sigma} + \frac{1}{2}\sum_{\substack{\boldsymbol{q}\neq 0\\ \boldsymbol{k}\boldsymbol{k}'\sigma\sigma'}} v_q\psi^{\dagger}_{\boldsymbol{k}+\boldsymbol{q}\sigma}\psi^{\dagger}_{\boldsymbol{k}'-\boldsymbol{q}\sigma'}\psi_{\boldsymbol{k}'\sigma'}\psi_{\boldsymbol{k}\sigma}, \quad (2)$$

where $\psi_{\boldsymbol{k}\sigma}$ and $\psi^{\dagger}_{\boldsymbol{k}\sigma}$ are the annihilation and creation operators for an electron with momentum $\boldsymbol{k}$ and spin $\sigma$, $\mu$ is the chemical potential, and $v_q = 4\pi e^2/q^2$ is the Coulomb interaction.

The central idea is to reorganize many-body perturbation theory around a variationally optimized screened interaction. Counterterms are introduced to preserve the exact physics of the original Hamiltonian, ensuring that the expansion remains unbiased. The diagrammatic series is then sampled as a computational graph, where counterterm contributions are obtained through Taylor-mode automatic differentiation. Further technical details of the VDMC method are given in Section SI of the Supplemental Material (SM).

Our implementation incorporates automated high-order renormalization and GPU-accelerated integration routines [42], allowing efficient evaluation of high-dimensional diagrams up to sixth order. This combination provides unprecedented computational reach for effective field theories in strongly interacting systems.

Systematic cancellation between same-order expansion terms generated when the constituent quantities of a physical observable are multiplied accelerates the convergence of the final result. For the Landau parameters, this mechanism is shown explicitly in Eqs. (S2) and (S3) and Fig. S1 of the SM: the combined observable converges faster than the separate quasiparticle-weight, effective-mass, and vertex ingredients. For instance, at $r_s = 4$ the combined parameters converge by sixth order, with uncertainties estimated from the spread of the last three expansion orders.

## Landau Parameters and Screening Crossover

The 3D UEG is characterized by the density parameter, the Wigner–Seitz radius $r_s = (3/4\pi n)^{1/3}$ and the reduced temperature $\Theta = T/T_{\mathrm{F}}$. We investigate $r_s = 1$–$6$ in the low-temperature, degenerate Fermi-liquid regime, using $\Theta = 0.025$ and $0.05$. The corresponding physical temperature scale is set by the Fermi temperature $T_{\mathrm{F}} = \hbar^2 k_{\mathrm{F}}^2/(2m_e k_{\mathrm{B}})$, where the Fermi momentum is $k_{\mathrm{F}} = (9\pi/4)^{1/3}/(a_0 r_s)$, giving $T_{\mathrm{F}} \simeq 5.82\times 10^5/r_s^2$ K. This scale shows that the lowest temperatures reached in our calculations are of order room temperature even at $r_s = 6$. Within Landau–Silin theory [50,51], the effective short-range interaction between quasiparticles on the Fermi surface $f_{\sigma\sigma'}(\theta)$, which encapsulates many-body correlations, is obtained from the small-frequency and long-wavelength limit of the four-point vertex diagram $\Gamma_4$ as

$$f_{\sigma\sigma'}(\theta) = z^2\lim_{\boldsymbol{q}\to 0}[\Gamma^{\sigma\sigma'}_4(\boldsymbol{k}_1\omega_{-1},\boldsymbol{k}_2\omega_0;\boldsymbol{k}_1+\boldsymbol{q}\omega_0) - v_q]. \quad (3)$$

Here, $\theta$ is the angle between the incoming momenta $\boldsymbol{k}_1$ and $\boldsymbol{k}_2$ on the Fermi surface, $\omega_0 = \mathrm{i}\pi T$ and $\omega_{-1} = -\mathrm{i}\pi T$ are fermionic Matsubara frequencies, and $z$ is the quasiparticle renormalization factor derived from the self-energy [42]. Meanwhile, the two-electron scattering amplitude, $a_{\sigma\sigma'}(\theta,\phi)$, is related to the four-point vertex for elastic scattering of quasiparticles on the Fermi shell as:

$$a_{\sigma\sigma'}(\theta,\phi) = z^2\Gamma^{\sigma\sigma'}_4(\boldsymbol{k}_1\omega_0,\boldsymbol{k}_2\omega_0;\boldsymbol{k}_3\omega_0), \quad (4)$$

where $\phi$ is the angle between the plane defined by $(\boldsymbol{k}_1,\boldsymbol{k}_2)$ and the plane defined by the outgoing momenta $(\boldsymbol{k}_3,\boldsymbol{k}_4)$.

Figure 2 shows the dimensionless spin-symmetric and antisymmetric Landau parameters $F^{\mathrm{s,a}}_l$ $(l = 0,1,2)$ as functions of $r_s$. These parameters, which characterize fundamental many-body interactions in the electron gas, are defined as Legendre components of the dimensionless quasiparticle interaction $F^{\mathrm{s,a}}(\theta) = (F_{\uparrow\uparrow}(\theta) \pm F_{\uparrow\downarrow}(\theta))/2$ with $F_{\sigma\sigma'}(\theta) = N^*_{\mathrm{F}} f_{\sigma\sigma'}(\theta)$, where $N^*_{\mathrm{F}} = \frac{m^*}{m}N_{\mathrm{F}}$ is the renormalized density of states at the Fermi surface.

One pivotal observation is the linear decrease of the compressibility-related parameter: $F^{\mathrm{s}}_0 \approx -0.17 r_s$. This behavior drives the Coulomb screening effect from "underscreening" to "overscreening", with the crossover occurring at $F^{\mathrm{s}}_0 = -1$ where the inverse compressibility (equivalently, the bulk modulus) vanishes and the ion-ion interaction becomes effectively attractive at large distances [47,52]. Our calculations show that this crossover occurs near $r_s^{\mathrm{c}} \approx 5.7$, close to the previous theoretical prediction of $r_s = 5.25$ in Ref. [46].* Importantly, the higher-order Landau parameters remain significantly smaller than $F^{\mathrm{s}}_0$, demonstrating the rapid convergence of the Legendre expansion. For comparison, figure 2 also shows $F^{\mathrm{s}}_0$ obtained from the RPA vertex

*A further discussion of this crossover phenomenon, including numerical results for the density response function and the ion-ion interaction, is provided in Section IV of the SM.

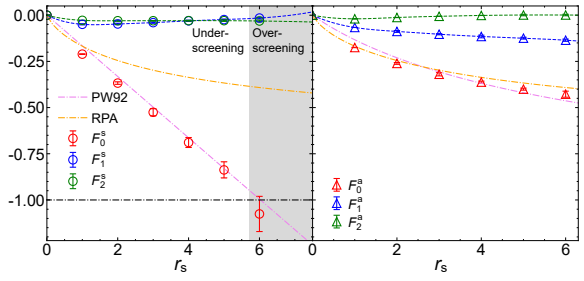


**Fig. 2.** Numerical results of the symmetric (left panel) and antisymmetric (right panel) Landau parameters versus $r_s$, confirming the rapid convergence of the Legendre expansion. The linear decrease of $F_0^s$ with $r_s$, which approaches $-1$ at $r_s^c \approx 5.7$, reveals the crossover of the Coulomb screening effect from underscreening to overscreening [46]. For comparison, the orange dash-dot line shows the $F_0$ calculated from the RPA vertex. The violet dash-dot line presents the dimensionless static XC kernel $f_{XC}(q=0)N_F$ for the UEG derived from the PW92 energy functional [49], demonstrating the approximate equality of the XC kernel and the zeroth Landau parameter. The corresponding numerical data are listed in Table S1 of the SM.

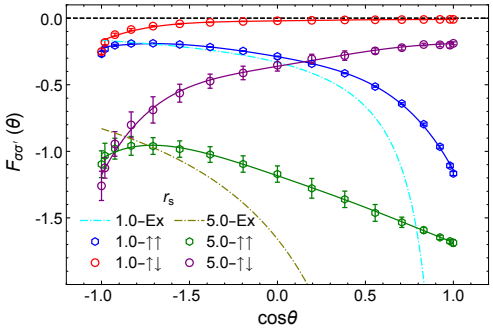


**Fig. 3.** Angle-resolved Landau quasiparticle interaction for $r_s = 1, 5$ with parallel and antiparallel spins. The dotted-dashed line represents the bare exchange Coulomb interaction. The larger deviation from the bare interaction for $r_s = 5$ indicates that Coulomb screening increases as the electron density decreases.

and the dimensionless zero-momentum static XC kernel $f_{XC}^{\pm}(q=0)N_F$ derived from the PW92 energy functional [49]. The PW92 XC kernels agree well with our numerically extracted $F_0^{s,a}$, confirming the approximate equality between the static zero-transfer-momentum XC kernel and the corresponding Landau parameters as

$$f_{XC}^{\pm}(q=0)N_F \approx F_0^{s,a}, \tag{5}$$

for $r_s$ in the metallic regime—a relation specific to the homogeneous electron liquid and not generally shared by arbitrary Fermi liquids. The theoretical insights of this relation will be discussed in Section III in the SM.

In addition, the parameter $F_1^s$ plays a crucial role in determining the effective mass $m^*$ through the relation $m^*/m = 1 + F_1^s$, where $m$ represents the bare electron mass. Our finding that $F_1^s$ remains small ($|F_1^s| \lesssim 0.05$) throughout the metallic density regime confirms the variational Monte Carlo and VDMC results [32,53,54] that the effective mass approximately equals the bare mass in this regime.

Figure 3 displays the angle-resolved Landau quasiparticle interaction $F_{\sigma\sigma'}(\theta)$ versus $\cos\theta$ at $r_s = 1$ and 5 for both parallel ($\uparrow\uparrow$) and antiparallel spin ($\uparrow\downarrow$) configurations, together with the bare exchange Coulomb interaction $W_{Ex}(\boldsymbol{k}_1, \boldsymbol{k}_2) = -N_F v(|\boldsymbol{k}_1 - \boldsymbol{k}_2|)$ for reference. Two features of the many body effect are observed through our data. First, in the parallel-spin channel, $F_{\uparrow\uparrow}(\theta)$ deviates from the bare exchange primarily at small angles at $r_s = 1$ but becomes smoothly angle-dependent at $r_s = 5$ with deviations across all angles, indicating enhanced screening and an increasingly local quasiparticle interaction as the density decreases—a trend that naturally justifies an LDA treatment of the charge channel. Second, the antiparallel-spin channel $F_{\uparrow\downarrow}(\theta)$, which receives no bare short-range contribution, develops a pronounced minimum at $\theta = \pi$ associated with dynamical screening that drives Cooper-pairing instability [55].

## Scattering Amplitude and the sKO$^+$ Ansatz

Figure 4 presents the dimensionless two-electron scattering amplitude, $A^{\sigma\sigma'}(\theta,\phi) = N_F^* a_{\sigma\sigma'}(\theta,\phi)$, for the UEG. We analyze the forward-scattering ($\phi = 0$) and Cooper ($\theta = \pi$) channels at $r_s = 1$ and 5 for $T/T_F = 0.025$, and include $T/T_F = 0.05$ for $r_s = 5$. Comparison of these datasets demonstrates that our results have reached the zero-temperature limit within error bars, except for the Cooper channel divergence caused by the Tolmachev singularity [55]. Crucially, as this singularity is confined to a phase space of measure zero, it has a negligible impact on Fermi-surface integrals in general. Based on these validated numerical results, we propose the sKO$^+$ ansatz: it is based on the charge KO interaction within LDA, which treats the symmetric (antisymmetric) XC kernel $f_{XC}^{\pm}(q) \approx f_{XC}^{\pm}(0) (:= f_{XC}^{\pm}$ as mentioned previously), supplemented by an s-wave correction $\delta R$ for the antiparallel spin configuration as presented in Eq. (1).

To motivate the structure of the proposed sKO$^+$ ansatz, we first benchmark common theoretical models against our high-precision VDMC data in Fig. 4. (i) RPA: the simplest case of Eq. (1), where the XC effect is entirely neglected as $f_{XC}^{+}(0) = 0$ and $\delta R = 0$, is clearly inadequate, especially in the low-density regime ($r_s \sim 5$). (ii) KO$^+$: the charge-channel KO interaction, which corresponds to $\delta R = 0$ in Eq. (1), agrees well with numerical results in the forward-scattering channel but deviates significantly approaching the Cooper channel. (iii) KO$^{\pm}$: the full KO interaction, which further incorporates the spin-channel interaction

$$R_- = \hat{\sigma}\cdot\hat{\sigma}'\left[\frac{f_{XC}^-}{1 - f_{XC}^- \Pi_0(q)} - f_{XC}^-\right],$$

performs worse as $r_s$ increases, particularly for antiparallel spins [Figs. 4(d) and 4(f)]. The superior performance of KO$^+$ over KO$^{\pm}$ suggests that spin interactions are implicitly captured via the exchange component of the charge interaction, without requiring explicit spin-channel terms. (iv) The s–p approximation [18,19]: it truncates scattering to s- and p-wave channels, which matches our numerical data well, confirming that higher-order partial waves are negligible. However, this approximation is restricted to the Fermi surface and fails to provide a complete effective interaction at other energy scales.

The relatively good performance of KO$^+$ indicates that the dominant long-range charge screening is already captured, so the remaining discrepancy can be treated as a residual short-range contribution. We therefore analyze the residual scattering amplitude

$$\delta A^{\sigma\sigma'}(\theta,\phi) = A^{\sigma\sigma'}_{VDMC}(\theta,\phi) - A^{\sigma\sigma'}_{KO^+}(\theta,\phi), \tag{6}$$

and expand it in the orthogonal Fermi-surface basis [56]

$$\delta A^{\sigma\sigma'}(\theta,\phi) = \sum_{k=0}^{\infty}\sum_{l=0}^{k} \delta A_{lk}^{\sigma\sigma'} X_{lk}(\theta,\phi). \tag{7}$$

As summarized in Fig. 5 (with further details in Section V of the SM), this expansion shows that the residual is negligible for parallel spins and is dominated by the $(l,k) = (0,0)$ and $(0,1)$ components for antiparallel spins. Guided by this clear structure, we formulate the sKO$^+$ effective interaction in Eq. (1). This construction keeps the exact long-range Coulomb screening inherited from KO$^+$ while correcting the antiparallel-spin deficit through a minimal contact-interaction ansatz inspired by effective field theory for dilute Fermi gases [57,58] with $C_0$ and $C_2$ related to the s-wave scattering length and effective range. As shown by the solid curves in Fig. 4, the resulting sKO$^+$ reproduces the full VDMC scattering amplitude on the Fermi surface across all tested densities, channels, and spin configurations, thereby resolving the Fermi-surface deficiencies of the conventional models.

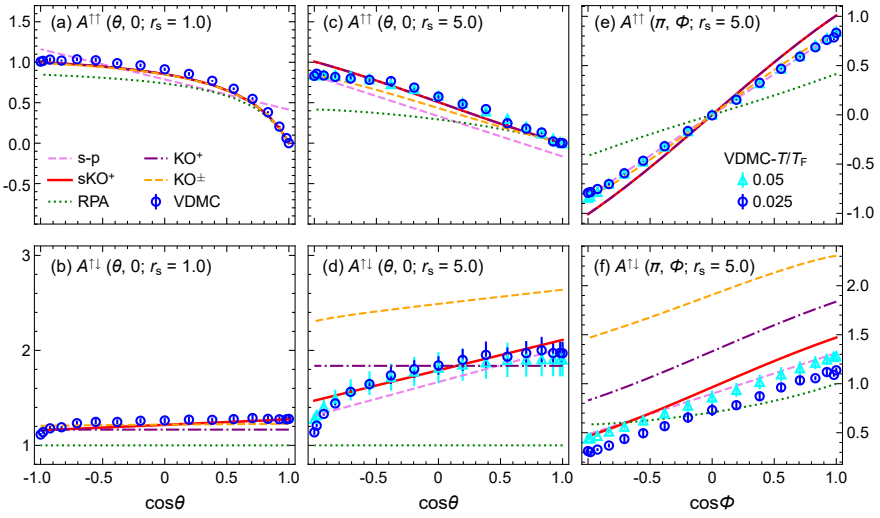


**Fig. 4.** The dimensionless two-electron scattering amplitude $A^{\sigma\sigma'}(\theta,\phi)$ for parallel ($\uparrow\uparrow$, top row) and antiparallel ($\uparrow\downarrow$, bottom row) spins at $r_s = 1$ and $r_s = 5$ at $T/T_F = 0.025$. Panels (a)–(d) show the forward scattering channel ($\phi = 0$). Panels (e)–(f) show the Cooper channel ($\theta = \pi$). Our VDMC results (symbols) are compared against several theoretical models. The solid curves show the sKO$^+$ ansatz obtained from the residual analysis of our VDMC data relative to the KO$^+$ interaction (see Fig. 5 and main text), agreeing well with the numerical results. For $r_s = 5$, numerical results at $T/T_F = 0.05$ are also plotted. The divergence of the scattering amplitude at both low temperatures in the Cooper channel is consistent with the expected logarithmic divergence of the four-point vertex function as $T \to 0$ [55].

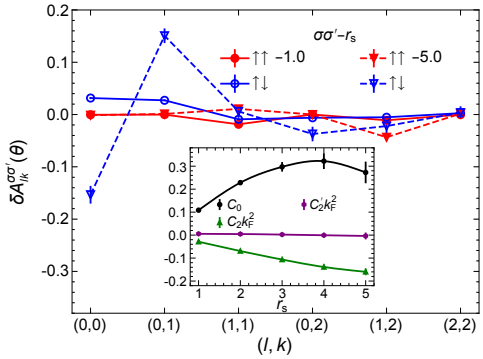


**Fig. 5.** General polynomial expansion [56] of the residual scattering amplitude beyond the KO$^+$ ansatz. The residual is negligible for parallel spins and is dominated by the s-wave components for antiparallel spins. The inset sketches the resulting parametrization of $\delta R$ in Eq. (1), where $C_0$ and $C_2$ correspond to the s-wave scattering length and effective range, while the higher-order p-wave correction $C_2'$ is negligible.

## Thermal Resistivity in Simple Metals

We now apply our calculated scattering amplitudes to compute macroscopic transport properties [6,10,59], enabling a direct validation of our numerical results against experimental benchmarks. In simple metals, deviations from the Wiedemann–Franz law—which asserts that the electrical resistivity $\rho$ and thermal resistivity $W$ relate to a universal constant $L_0$ via the equation $\rho/(WT) = L_0$—are experimentally observed, particularly above the Debye temperature [60]. This deviation manifests as an additional thermal resistance with a linear temperature dependence, identified as the electron–electron scattering contribution, $W_{ee}$ [21–24]. However, a precise theoretical description has remained elusive: conventional first-principles DFT typically struggles to capture such dynamical scattering processes, while standard many-body approximations like RPA and the original KO$^\pm$ interaction fail to reproduce the experimental magnitude—yielding significant underestimates and overestimates, respectively (Fig. 1). By contrast, utilizing the full angular dependence of our *ab initio* scattering amplitudes (see Section SVI in the SM), our VDMC calculations achieve excellent agreement with measurements for simple metals (Al, Na, K, Rb). For these nearly-free-electron metals, band-mass and core-polarization corrections are small. Therefore, the crystal structures and the DFT bands are not included at this stage as a density-parametrized UEG benchmark and these metals are only represented by the corresponding valence-electron density parameter $r_s$, allowing our results to be compared directly with the measured electron–electron thermal resistivity. Remarkably, this agreement is faithfully reproduced by the computationally efficient sKO$^+$ ansatz, highlighting its promise for incorporating accurate electron–electron scattering into future material-specific first-principles transport calculations. Complementing these macroscopic resistivity results, we also present the quasiparticle scattering rate in the inset of Fig. 1, providing the fundamental timescale governing these transport dynamics [6,10].

## Discussion

In summary, we have presented high-precision *ab initio* calculations of the four-point vertex function of the 3D UEG using our developed VDMC framework. The extracted Landau parameters validate LDA and reveal how the dominant $F_0^s$ drives the system from underscreening toward overscreening as the density decreases. Guided by a residual analysis of our scattering amplitudes against the KO$^+$ interaction, we have established the sKO$^+$ ansatz: a charge-channel KO interaction in LDA supplemented by a minimal antiparallel-spin s-wave correction. The sufficiency of such short-range corrections parallels recent findings that imperfect screening at short distances is essential for capturing the physics of the low-density regime [61].

The excellent agreement among experimental thermal-resistivity measurements, our direct VDMC calculations, and the sKO$^+$ ansatz demonstrates that this simple effective interaction is both quantitatively accurate and predictive. Its closed form is built from the static XC kernel and two short-range coefficients tabulated from UEG data, making it straightforward to use as an electron–electron kernel in TDDFT or related dielectric-response calculations, where the long-wavelength charge response must be retained while local correlation effects are improved. Because the same interaction reproduces the full Fermi-surface scattering amplitude, it also provides a controlled input for Eliashberg- and Boltzmann-type calculations, in which pairing tendencies, quasiparticle lifetimes, and electron–electron-limited thermal transport depend directly on the angular structure of the scattering amplitude. More generally, the structure of sKO$^+$ may help guide the construction of low-energy effective field theories for correlated electron systems.

Looking forward, our VDMC data offer crucial numerical benchmarks for emerging experimental techniques that probe two-particle correlations in materials [15–17], and pave the way for next-generation

*ab initio* material-specific extensions, where downfolding the UEG vertex function may provide one route toward constructing accurate effective Hamiltonians. Extending this direction beyond the nearly-free-electron limit will require a material-specific treatment of band structure and core-electron effects, for example through effective-field-theory approaches to band renormalization [62].

## Acknowledgments

K.C. extends sincere thanks to Boris Svistunov and Carl A. Kukkonen for their valuable discussions. K. C. was supported by the National Key Research and Development Program of China (Grant No. 2024YFA1408604), the National Natural Science Foundation of China (Grant Nos. 12474245 and 12447103), and the GHfund A (Grant No. 202407010637). Z.L., P.H., and Y.D. were supported by the National Natural Science Foundation of China (Grant No. 12275263), the Quantum Science and Technology National Science and Technology Major Project (Grant No. 2021ZD0301900), and the Natural Science Foundation of Fujian Province of China (Grant No. 2023J02032).

## References

[1] Alexandradinata A, Armitage N P, Baydin A, Bi W, Cao Y, Changlani H J, Chertkov E, da Silva Neto E H, Delacretaz L, Baggari I E, Ferguson G M, Gannon W J, Ghorashi S A A, Goodge B H, Goulko O, Grissonnanche G, Hallas A, Hayes I M, He Y, Huang E W, Kogar A, Kumah D, Lee J Y, Legros A, Mahmood F, Maximenko Y, Pellatz N, Polshyn H, Sarkar T, Scheie A, Seyler K L, Shi Z, Skinner B, Steinke L, Thirunavukkuarasu K, Trevisan T V, Vogl M, Volkov P A, Wang Y, Wang Y, Wei D, Wei K, Yang S, Zhang X, Zhang Y H, Zhao L, and Zong A 2025 *SciPost Phys. Comm. Rep.* **8**
[2] Dagotto E 1994 *Rev. Mod. Phys.* **66** 763
[3] Greene R L, Mandal P R, Poniatowski N R, and Sarkar T 2020 *Annu. Rev. Condens. Matter Phys.* **11** 213
[4] Hasan M Z and Kane C L 2010 *Rev. Mod. Phys.* **82** 3045
[5] Loos P F and Gill P M W 2016 *Wiley Interdiscip. Rev. Comput. Mol. Sci.* **6** 410
[6] Mahan G D 2013 *Many-particle physics* (Springer New York, NY)
[7] Abrikosov A A, Gorkov L P, and Dzyaloshinski I E 2012 *Methods of quantum field theory in statistical physics* (Courier Corporation)
[8] Negele J W 2018 *Quantum many-particle systems* (CRC Press)
[9] Bardeen J, Cooper L N, and Schrieffer J R 1957 *Phys. Rev.* **108** 1175
[10] Brooker G A and Sykes J 1968 *Phys. Rev. Lett.* **21** 279
[11] Galler A, Thunström P, Gunacker P, Tomczak J M, and Held K 2017 *Phys. Rev. B* **95** 115107
[12] Kaufmann J, Eckhardt C, Pickem M, Kitatani M, Kauch A, and Held K 2021 *Phys. Rev. B* **103** 035120
[13] Cunningham B 2025 *Phys. Rev. B* **112** 115153
[14] Zang J, Medvidović M, Kiese D, Di Sante D, Sengupta A M, and Millis A J 2024 *Mach. Learn. Sci. Technol.* **5** 045076
[15] Devereaux T P, Claassen M, Huang X X, Zaletel M, Moore J E, Morr D, Mahmood F, Abbamonte P, and Shen Z X 2023 *Phys. Rev. B* **108** 165134
[16] Su Y and Zhang C 2020 *Phys. Rev. B* **101** 205110
[17] Fresch E, Camargo F V, Shen Q, Bellora C C, Pullerits T, Engel G S, Cerullo G, and Collini E 2023 *Nat. Rev. Methods Primers* **3** 84
[18] Dy K S and Pethick C J 1969 *Phys. Rev.* **185** 373
[19] MacDonald A H and Geldart D J W 1980 *J. Phys. F: Met. Phys.* **10** 677
[20] Kukkonen C A and Overhauser A W 1979 *Phys. Rev. B* **20** 550
[21] Cook J G, Meer M P V d, and Laubitz M J 1972 *Can. J. Phys.* **50** 1386
[22] Laubitz M J and Cook J G 1973 *Phys. Rev. B* **7** 2867
[23] Cook J G 1979 *Can. J. Phys.* **57** 1216
[24] Uher C 2004 Thermal Conductivity of Metals (Springer, Boston, MA) p. 21
[25] Levy B, Sinvani M, and Greenfield A J 1979 *Phys. Rev. Lett.* **43** 1822
[26] van Kempen H, Ribot J H J M, and Wyder P 1981 *J. Phys. F: Met. Phys.* **11** 597
[27] Shaffer N R and Starrett C E 2020 *Phys. Rev. E* **101** 053204
[28] Lindhard J 1954 *Kgl. Danske Videnskab. Selskab Mat.-Fys. Medd.* **28**
[29] Kukkonen C A and Smith H 1973 *Phys. Rev. B* **8** 4601
[30] Kukkonen C A and Wilkins J W 1979 *Phys. Rev. B* **19** 6075
[31] Chen K and Haule K 2019 *Nat. Commun.* **10** 3725
[32] Haule K and Chen K 2022 *Sci. Rep.* **12** 2294
[33] Prokof'ev N V and Svistunov B V 1998 *Phys. Rev. Lett.* **81** 2514
[34] Prokof'ev N and Svistunov B 2008 *Phys. Rev. B* **77** 020408
[35] Kozik E, Ferrero M, and Georges A 2015 *Phys. Rev. Lett.* **114** 156402
[36] Rossi R 2017 *Phys. Rev. Lett.* **119** 045701
[37] Prokof'ev N and Svistunov B 2007 *Phys. Rev. Lett.* **99** 250201
[38] Rossi R, Ohgoe T, Van Houcke K, and Werner F 2018 *Phys. Rev. Lett.* **121** 130405
[39] Van Houcke K, Werner F, Kozik E, Prokof'ev N V, Svistunov B V, Ku M, Sommer A, Cheuk L, Schirotzek A, and Zwierlein M 2012 *Nat. Phys.* **8** 366
[40] Brolli S, Barbieri C, and Vigezzi E 2025 *Phys. Rev. Lett.* **134** 182502
[41] Wang Y and Haule K 2025 *Phys. Rev. Lett.* **135** 176501
[42] Hou P, Wang T, Cerkoney D, Cai X, Li Z, Deng Y, Wang L, and Chen K 2025 arXiv: 2403.18840 [hep-th]
[43] Li Z, Hou P, Deng Y, and Chen K 2025 *Phys. Rev. B* **111** 155132
[44] Hou P C, Wang B Z, Haule K, Deng Y, and Chen K 2022 *Phys. Rev. B* **106** L081126
[45] Chen K 2024 arXiv: 2404.15844 [cond-mat.str-el]
[46] Takada Y 1991 *Phys. Rev. B* **43** 5979
[47] Matsuda K, Tamura K, and Inui M 2007 *Phys. Rev. Lett.* **98** 096401
[48] Takayanagi K and Lipparini E 1997 *Phys. Rev. B* **56** 4872
[49] Perdew J P and Wang Y 1992 *Phys. Rev. B* **45** 13244
[50] Silin V 1958 *Sov. Phys. JETP* **6** 387
[51] Silin V 1958 *Sov. Phys. JETP* **6** 33
[52] Maebashi H and Takada Y 2007 arXiv: 0706.4001 [cond-mat.other]
[53] Takada Y 2024 *Phys. Rev. B* **110** 085132
[54] Holzmann M, Bernu B, Olevano V, Martin R M, and Ceperley D M 2009 *Phys. Rev. B* **79** 041308
[55] Cai X, Wang T, Prokof'ev N V, Svistunov B V, and Chen K 2022 *Phys. Rev. B* **106** L220502
[56] Pfitzner M 1985 *J. Low Temp. Phys.* **61** 141
[57] Hammer H W and Furnstahl R 2000 *Nucl. Phys. A* **678** 277
[58] Wellenhofer C, Drischler C, and Schwenk A 2020 *Phys. Lett. B* **802** 135247
[59] Jensen H H, Smith H, and Wilkins J W 1969 *Phys. Rev.* **185** 323
[60] Kittel C and McEuen P 2018 *Introduction to solid state physics* (John Wiley & Sons)
[61] Koskelo J, Reining L, and Gatti M 2025 *Phys. Rev. Lett.* **134** 046402
[62] Cai X, Wang H, and Chen K 2026 arXiv: 2604.25199 [cond-mat.mtrl-sci]